Technical Note

Design and fabrication of a personalized anthropomorphic phantom using 3D printing and tissue equivalent materials

Fuquan Zhang[1#], Haozhao Zhang[1#], Huihui Zhao[1], Zhengzhong He[2], Liting Shi[1], Yaoyao He[1], Nan Ju[1], Yi Rong[3], Jianfeng Qiu[1]

[1]Medical Engineering and Technical Center, Taishan Medical University, Taian 271000, China; [2]Radiation Department, Hubei Cancer Hospital, Wuhan 430079, China; [3]Department of Radiation Oncology, University of California Davis Comprehensive Cancer Center, Sacramento, CA, USA

[#]These authors contributed equally to this work.

Correspondence to: Jianfeng Qiu, PhD. Department of Radiology, Taishan Medical University, No. 619, Changcheng Road, Taian 271016, China. Email: jfqiu100@gmail.com; Yi Rong, PhD. Department of Radiation Oncology, University of California Davis Comprehensive Cancer Center, 4501 X Street, Suite 0152, Sacramento, CA 95817, USA. Email: yrong@ucdavis.edu.

Abstract: To fabricate an individualized anthropomorphic lung phantom with tissue-equivalent radiation attenuation properties using a cost-effective three-dimensional (3D) printing technique. Based on anonymized human chest CT images, the phantom contained a 3D-printed skin shell, filled with tissue equivalent materials with similar radiation attenuation characteristics. The filling materials were a mixture of $CaCO_3$, MgO, agarose, NaCl, pearl powder and silica gel. The dose calculation accuracy of different treatment planning system (TPS) algorithms was validated and compared with the ion chamber measurements in the phantom, including tumor and surrounding normal tissues. The chest phantom was shown to represent a human's chest in terms of radiation attenuation property and human anatomy. The Hounsfield unit ranges were −60 to −100, 20 to 60, and 120 to 300 for fat, muscle, and bone, respectively. The actual measured values of the ionization chamber were 213.7 cGy for the tumor, 53.85 cGy for normal lung tissue, and 4.1 cGy for the spinal cord, compared to 214.1, 55.2, and 4.5 cGy, respectively, with use of the Monte Carlo algorithm in TPS. The application of 3D printing in anthropomorphic phantoms can improve personalized medical need and efficiency with reduce costs thus, can be used for radiation dose verification.

Keywords: 3D printing; simulation phantom; personalized

Submitted Jun 13, 2018. Accepted for publication Jul 21, 2018.
doi: 10.21037/qims.2018.08.01
View this article at: http://dx.doi.org/10.21037/qims.2018.08.01

Introduction

The goal of radiotherapy is to deliver the highest possible dose of radiation to a tumor while minimizing normal tissue toxicities (1). The dose distribution needs to be calculated with a radiation treatment planning system (TPS), and verified by quality assurance (QA) tests (2). In recent years, some researchers used three-dimensional (3D) printing technology to make phantoms for QA and dose verification. Similar ideas are used for fabricating a kidney phantom reported by Adams et al, which used agarose in phantom production (3). Ehler *et al.* used fused deposition printing technology to make anthropomorphic phantoms for radiation therapy dose measurements (4).

By using a PolyJet printer, Mayer *et al.* presented a chest phantom for detection of dose inside and outside a moving tumor and in lung tissues (5). Menikou *et al.* reported a 3D printed MRI compatible head phantom (6). Adams *et al.* further constructed soft phantoms using a novel technique that combined 3D wax printing and polymer molding. Similar method

was also found in the studies on bone and lung tissues, MR images, and small animal experiments (7-11). Despite these advanced technologies, these previously reported methods are complicated and hard to be practically adopted for clinical use. In addition, the tissue-equivalency of previously used materials has not been proved in terms of radiation attenuation. The clinical applications of various anthropomorphic phantoms include equipment calibration, QA, dose verification, teaching, surgical guidance, etc. (12-15). For these purposes, they should be designed with similar human anatomy and attenuation characteristics (16). However, the tissue equivalent materials are not readily available for 3D printing (17,18).

We herein proposed a formula that can produce adequate tissue-equivalency in terms of radiological attenuation and dose deposition. We also fabricated a chest phantom via 3D printing technique, and filled with the proposed materials to simulate soft tissue and fat. The purpose of our study is to create an anthropomorphic chest phantom with similar human anatomy and radiation attenuation properties of individual patient.

Materials and methods

3D phantom design

An anonymized chest CT was obtained from the Department of Radiology, Hubei Cancer Hospital using the Brilliance CT scanner (Philips, Netherlands, 256-slice spiral CT, pitch value 0.27). The scanning parameters are as follows: tube voltage 120 kVp, current 260 mAs, slice thickness 0.5 mm, a total of 596 2D axial slices. The DICOM (Digital Imaging and Communications in Medicine) images were imported into Mimics Research 17.0 image analysis software (Materialize, Belgium). The chest phantom was divided into ribs, scapula, sternal angle, fat tissue, muscle tissue, lung tissue and lesion. Based on the image, each part of the bones and tissues were segmented and 3D reconstructed.

The models were created from the CT images in the Magic 10.0 software (Materialize, Belgium). The 3D models of fat tissue shell, lung tissue shell, ribs, scapula, and sternum were transformed to Magic 10.0 software and processed with solid generation and noise reduction, as shown in *Figure 1*.

3D printing models and materials

The segmented mesh files for the chest shell (mentioned in section "3D phantom design") were converted into the Standard Tessellation Language (STL) format for 3D printing. The material used in printing the fat and chest wall shell is acrylonitrile butadiene styrene (ABS). The radiation equivalent material of ribs, sternum angle and scapula was made with modified resin polymer material (8). The printed phantom shell is shown in *Figure 2*.

Selection of radiation equivalent materials

Various equivalent materials and blending ratios were selected via CT equivalent test (19,20). These materials were further tested and modified in our study to improve tissue equivalency for four tissue/organs, including fat, muscle, tumor lesion, and lung.

Figure 3 shows the comparison of unmodified and modified materials for all four tissue types. For fat tissue, the molted M3 wax was selected as the solvent, while $CaCO_3$ and MgO were used as solutes. For muscle tissue, water was chosen as the solvent, with agarose, NaCl, and pearl powder as solutes. For tumor lesions, water was used as solvent, with agarose, NaCl, and pearl powder as solute. For lung tissue, the foamed silica gel was made up of silica gel and curing agent by 1:1. Then, the silica gel was injected directly into the lung tissue shell. As shown in *Table 1*, the modified materials were in close approximation to human tissues in terms of CT numbers.

End-to-end testing for radiotherapy delivery

The acquired CT images of the phantom were imported into the TPS (Monaco 5.11, Elekta, Sweden). The target area was outlined and a 3D conformal radiotherapy plan with three beams was created using 6 MV X-rays, with a prescription dose of 2 Gy (3,5,21). The tumor dose was calculated in the TPS using the pencil beam convolution (PBC), collapse cone convolution (CCC) and Monte Carlo (MC) algorithms, respectively. The prescription dose was required to cover at least 95% of the planning tumor volume (PTV). The plan was delivered using a linear accelerator (Precise Treatment System™, Elekta, Sweden). The actual delivered dose to the PTV, lung, and spinal cord was measured using an ion chamber (UNIDOS E, PTW, Germany) and compared with the planned doses.

Results

Figure 4 shows the actual constructed chest phantom.

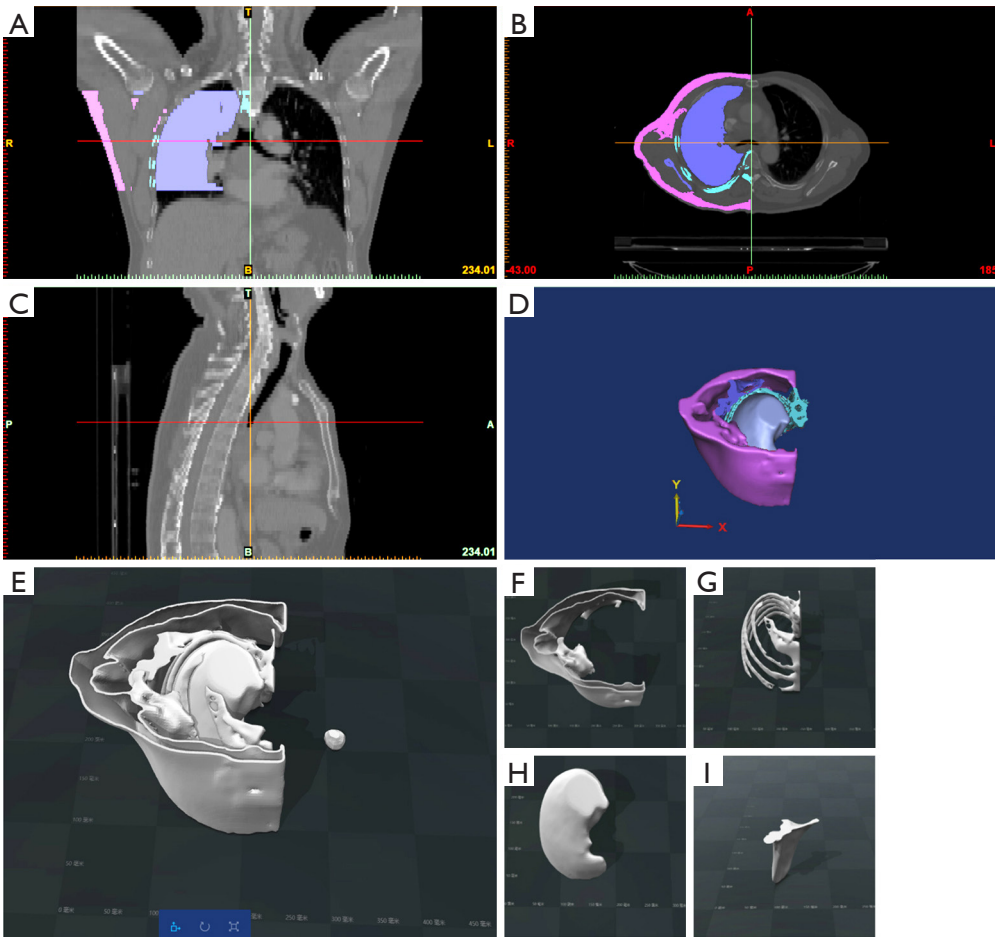

Figure 1 The regions of interest in patient CT data were processed by Mimics Research 17.0 (deep purple part represents lesions). (A) Coronal section; (B) transverse section; (C) sagittal plane; (D) 3D reconstruction; (E) the shell model of the muscle tissue opened up, the lung tissue shell model opened downward, and the rib model wrapped around the lung tissue model; (F) the shell model of muscle tissue (opening upwards); (G) the ribs and chest bone model; (H) the lung tissue shell model (opening downward); (I) the scapula model.

The phantom also went through the CT scan (*Figure 4A*) with the same parameters as the patient scanning. The CT image, as shown in *Figure 4B*, was compared with the patient chest scan *Figure 4C*. A CT image fusion of the phantom and the patient's chest is shown in *Figure 5*.

The CT image of the chest phantom is comparable to the human chest in morphology. *Table 2* shows comparison of CT numbers between phantom and patient images for fat tissue, muscle tissue, bone, and tumor. The differences were around 20 HU for fat, muscle and tumor, while around 55 HU on average for bone.

The dose comparison between calculated and measured methods is shown in *Table 3*. The ion-chamber measured doses were 213.7 cGy in tumor, 53.85 cGy in normal lung tissue, and 4.1 cGy in spinal cord. Meanwhile the calculated doses obtained by different algorithms were also shown. For the tumor, lung, and spinal cord, PBC reported 215.1, 52.5, and 1.9 cGy; CCC reported 214.6, 54.4, and 4.4 cGy; and MC reported 214.1, 55.2, and 4.5 cGy, respectively. The differences between measured and calculated dose were <1% for tumor, 1–2.5% for lung, and 7–9% for the spinal cord for both CCC and MC. The PBC algorithm is known to be in-accurate in dose calculation especially for lung region, thus showed higher discrepancies.

Discussion

With the development of 3D printing technology,

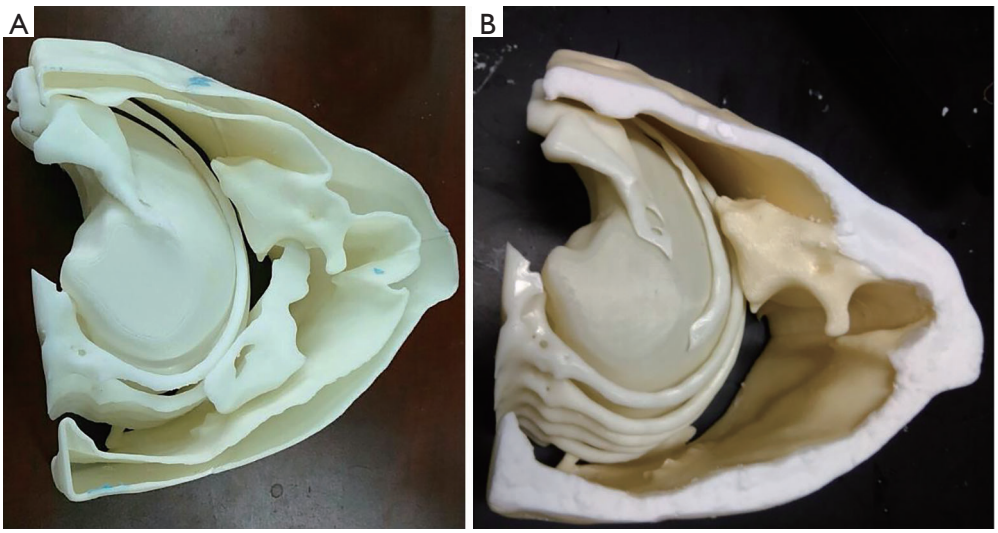

Figure 2 3D printed phantom shell. (A) Ribs, scapula, sternum angle, fat and lung tissue shells. (B) The phantom with fat tissue equivalent material.

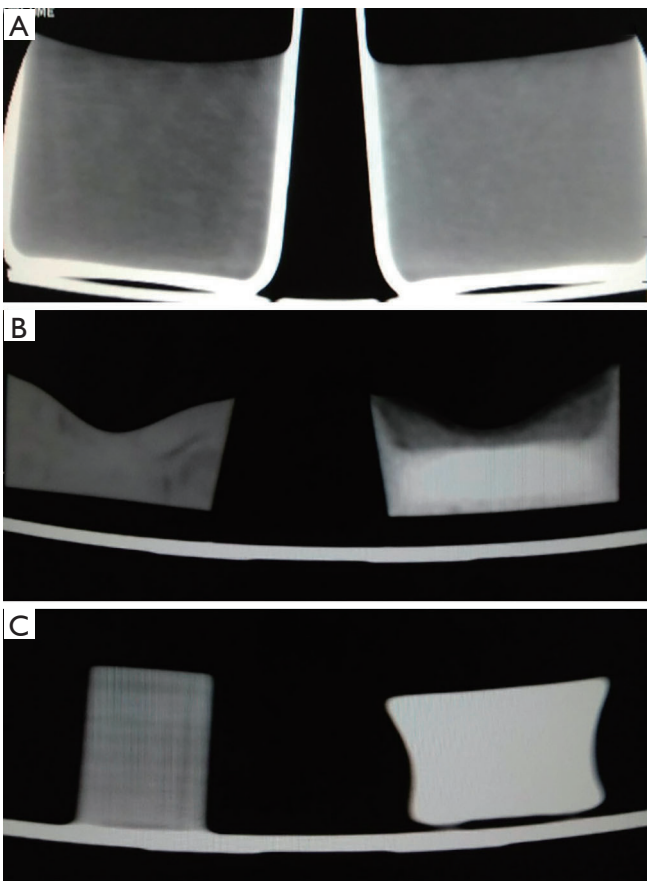

Figure 3 CT images of the unmodified materials (left column) and improved materials (right column). (A) Agarose, (B) wax and (C) printed materials.

Table 1 Comparison of unmodified materials and improved materials in CT numbers

CT number (HU)	Agarose	Wax	Printed materials
Unmodified materials	0±15	−150±20	−130±40
Modified materials	40±20	−100±30	160±40

phantoms can be manufactured in a simple and fast manner. In our experiments, a regular 3D printer can satisfy the 3D printing requirement for radiotherapy clinical use in printing personalized phantoms. Following the same method, other anatomical phantoms can be designed and fabricated, i.e., pelvis, breast, head, etc. Our end-to-end test in dose verification using the present phantom shows an immediate clinical use for individualized dose verification, especially for those complex plans requiring high precision. Through the phantom verification, we showed that both MC and CCC algorithms overestimated the dose in tumor, normal lung and spinal cord. The PBC overestimated the dose of tumor and underestimated the doses of normal lung tissues and spinal cord.

The fused deposition printing technology used in previous studies by Ehler *et al.* (4) and Bache *et al.* (11) may produce deformation during the production process. With that in consideration, we used photo-sensitive printers for our phantoms. Compared to the study by Mayer *et al.* (5), the CT numbers of our phantom is closer to actual human tissues. With the adjustable CT numbers of currently used

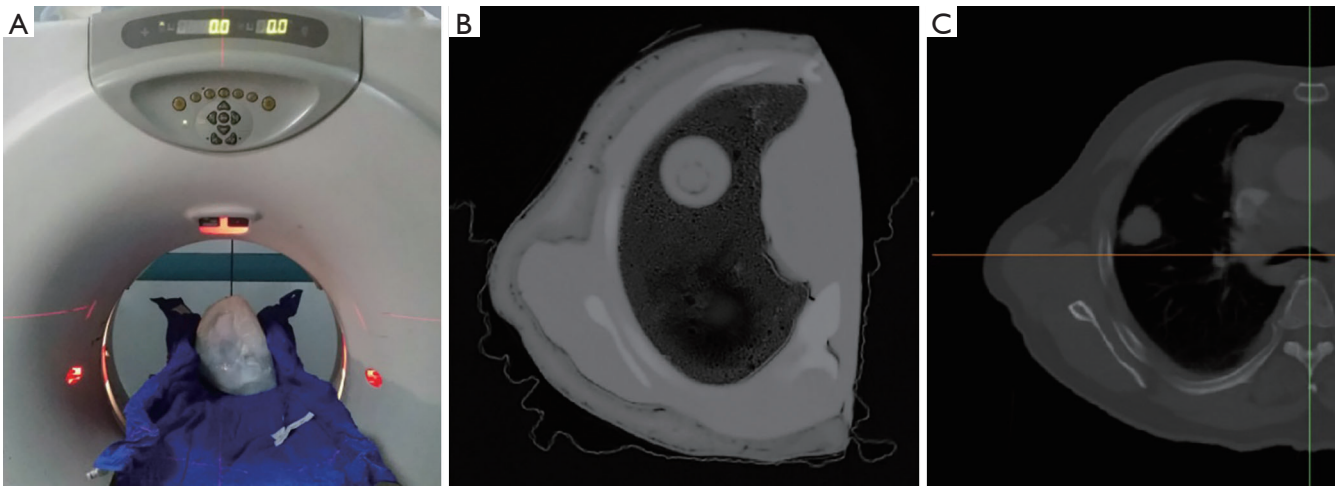

Figure 4 Verifying the imaging effect of chest phantom: (A) CT scanning of the phantom; (B) the CT image of the chest phantom; and (C) the CT image of the patient.

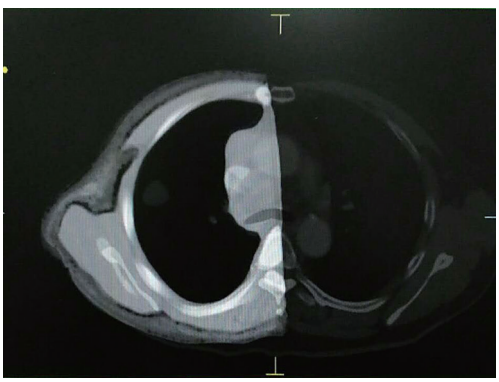

Figure 5 Image fusion of phantom and patient CT images.

Table 2 Comparison of the CT number of the phantom and patient images

CT number (HU)	Fat tissue	Muscle tissue	Bone	Tumor
Patient images	−80±20	60±30	265±135	55±25
Phantom images	−100±30	40±20	210±90	33±16

phantom materials, our future research will be producing various anatomical phantoms with tissue equivalency, such as liver phantom, kidney phantom, etc. Because of the simplicity of 3D printing phantoms, laboratory production is achieved without the need of complex industrial customization.

There are some limitations in our presented method. First, the 3D printer specifications restrict the size of a printable phantom. For larger size body regions (e.g., phantom), the phantom must be divided into several sections, before being printed and glued into a complete one. Second, the dissolution of the equivalent tissue materials requires evaluation and validation. The concentration of the solution affects uniformity and radiation attenuation property of the phantom. Third, the 3D printed phantom shell affects image quality and phantom stability. The 3D printing material of the shell is fragile, so it is necessary to accurately estimate the shell thickness according to the manufacturing method and experimental requirements. Although the production of such phantom is simple and convenient, further exploration and improvement are needed for large-scale clinical applications.

Conclusions

This study introduced a method of fabricating a lung phantom with anatomically accurate and X-ray attenuation equivalency to human tissues. The 3D printed thoracic phantom can be used for radiotherapy QA and dose verification.

Table 3 Comparison of the measured dose and calculated dose with TPS algorithms

Comparison subjects	Tumor tissue		Normal pulmonary tissue		Spinal cord	
	Dose (cGy)	Deviation (%)	Dose (cGy)	Deviation (%)	Dose (cGy)	Deviation (%)
Measurements	213.7		53.85		4.1	
PBC	215.1	0.66	52.5	–2.51	1.9	–53.66
CCC	214.6	0.42	54.4	1.02	4.4	7.32
MC	214.1	0.18	55.2	2.51	4.5	9.76

TPS, treatment planning system; PBC, pencil beam convolution; CCC, collapse cone convolution; MC, Monte Carlo.

Acknowledgements

Funding: This study is funded by National Key Research and Development Project (2016YFC0103400), and by the Shandong Province Key Research and Development Program (2017GSF218075). Jianfeng Qiu is supported by the Taishan Scholars Program of Shandong Province (TS201712065).

Footnote

Conflicts of Interest: The authors have no conflicts of interest to declare.

References

1. Oh SA, Kang MK, Kim SK, Ji WY. Comparison of IMRT and VMAT Techniques in Spine Stereotactic Radiosurgery with International Spine Radiosurgery Consortium Consensus Guidelines. Prog Med Phys 2013;24:145-53.
2. Yea JW, Park JW, Kim SK, Kim DY, Kim JG, Seo CY, Jeong WH, Jeong MY, Oh SA. Feasibility of a 3D-printed anthropomorphic patient-specific head phantom for patient-specific quality assurance of intensity-modulated radiotherapy. PLoS One 2017;12:e0181560.
3. Adams F, Tian Q, Mark A, Fritz B, Kramer L, Schlager D, Wetterauer U, Miernik A, Fischer P. Soft 3D-Printed Phantom of the Human Kidney with Collecting System. Ann Biomed Eng 2017;45:963-72.
4. Ehler ED, Barney BM, Higgins PD, Dusenbery KE. Patient specific 3D printed phantom for IMRT quality assurance. Phys Med Biol 2014;59:5763-73.
5. Mayer R, Liacouras P, Thomas A, Kang M, Lin L, Simone CB 2nd. 3D printer generated thorax phantom with mobile tumor for radiation dosimetry. Rev Sci Instrum 2015;86:074301.
6. Menikou G, Dadakova T, Pavlina M, Bock M, Damianou C. MRI compatible head phantom for ultrasound surgery. Ultrasonics 2015;57:144-52.
7. Rai R, Manton D, Jameson MG, Josan S, Barton MB, Holloway LC, Liney GP. 3D Printed Phantoms Mimicking Cortical Bone for the Assessment of Ultrashort Echo Time Magnetic Resonance Imaging. Med Phys 2018;45:758-66.
8. Ceh J, Youd T, Mastrovich Z, Peterson C, Khan S, Sasser TA, Sander IM, Doney J, Turner C, Leevy WM. Bismuth Infusion of ABS Enables Additive Manufacturing of Complex Radiological Phantoms and Shielding Equipment. Sensors (Basel) 2017;17:E459.
9. Jung J, Song SY, Yoon SM, Kwak J, Yoon K, Choi W, Jeong SY, Choi EK, Cho B. Verification of Accuracy of CyberKnife Tumor-tracking Radiation Therapy Using Patient-specific Lung Phantoms. Int J Radiat Oncol Biol Phys 2015;92:745-53.
10. Mitsouras D, Lee TC, Liacouras P, Ionita CN, Pietilla T, Maier SE, Mulkern RV. Three-dimensional printing of MRI-visible phantoms and MR image-guided therapy simulation. Magn Reson Med 2017;77:613-22.
11. Bache ST, Juang T, Belley MD, Koontz BF, Adamovics J, Yoshizumi TT, Kirsch DG, Oldham M. Investigating the accuracy of microstereotactic-body-radiotherapy utilizing anatomically accurate 3D printed rodent-morphic dosimeters. Med Phys 2015;42:846-55.
12. Goldman LW. Principles of CT: radiation dose and image quality. J Nucl Med Technol 2007;35:213-25.
13. Rowley LM, Bradley KM, Boardman P, Hallam A, Mcgowan DR. Optimization of Image Reconstruction for 90Y Selective Internal Radiotherapy on a Lutetium Yttrium Orthosilicate PET/CT System Using a Bayesian Penalized Likelihood Reconstruction Algorithm. J Nucl

Med 2017;58:658-64.
14. Mitsouras D, Liacouras P, Imanzadeh A, Giannopoulos AA, Cai T, Kumamaru KK, George E, Wake N, Caterson EJ, Pomahac B. Medical 3D Printing for the Radiologist. Radiographics 2015;35:1965-88.
15. Tai BL, Rooney D, Stephenson F, Liao PS, Sagher O, Shih AJ, Savastano LE. Development of a 3D-printed external ventricular drain placement simulator: technical note. J Neurosurg 2015;123:1070-6.
16. Jahnke P, Limberg FR, Gerbl A, Ardila Pardo GL, Braun VP, Hamm B, Scheel M. Radiopaque Three-dimensional Printing: A Method to Create Realistic CT Phantoms. Radiology 2017;282:569-75.
17. Tran-Gia J, Schlögl S, Lassmann M. Design and Fabrication of Kidney Phantoms for Internal Radiation Dosimetry Using 3D Printing Technology. J Nucl Med 2016;57:1998-2005.
18. Qian Z, Wang K, Liu S, Zhou X, Rajagopal V, Meduri C, Kauten JR, Chang YH, Wu C, Zhang C. Quantitative Prediction of Paravalvular Leak in Transcatheter Aortic Valve Replacement Based on Tissue-Mimicking 3D Printing. JACC Cardiovasc Imaging 2017;10:719-31.
19. Pogue BW, Patterson MS. Review of tissue simulating phantoms for optical spectroscopy, imaging and dosimetry. J Biomed Opt 2006;11:041102.
20. Park SH, Kang BK, Ji EL, Chun SW, Jang K, Kim YH, Mi AJ, Kim Y, Kang K, Lee NK. Design and Fabrication of a Thin-Walled Free-Form Scaffold on the Basis of Medical Image Data and a 3D Printed Template: Its Potential Use in Bile Duct Regeneration. ACS Appl Mater Interfaces 2017;9:12290-8.
21. Fisher M, Applegate C, Ryalat M, Laycock S, Hulse M, Emmens D, Bell D. Evaluation of 3-D Printed Immobilisation Shells for Head and Neck IMRT. Open J Radiol 2014;4:322-8.

Cite this article as: Zhang F, Zhang H, Zhao H, He Z, Shi L, He Y, Ju N, Rong Y, Qiu J. Design and fabrication of a personalized anthropomorphic phantom using 3D printing and tissue equivalent materials. Quant Imaging Med Surg 2019;9(1):94-100. doi: 10.21037/qims.2018.08.01

